Development of an Endurance Test Procedure for Vehicle Control Arm through Vehicle Dynamic Testing and Load Transfer Analysis

Nuurshafiqah Anuar[1], Syabillah Sulaiman [1,2]✉, Muhamad Asri Azizul[1,2], Shaiful Fadzil Zainal Abidin[1,2], Norirda Mohamed[1,2], Rahmah Mahmudin[1,2], Norhasikin Ismail[1,2]

[1]Faculty of Engineering Technology, Universiti Tun Hussein Onn Malaysia, 84600 Panchor, Muar, Johor, Malaysia.
[2]Vehicle Dynamic & Sustainable Development (VeDys) Focus Group, Universiti Tun Hussein Onn Malaysia, 84600 Panchor, Muar, Johor, Malaysia.

✉ syabillah@uthm.edu.my

Abstract

This research studies the forces applied to various vehicle control arms through different static and dynamic conditions during acceleration and braking condition. This study is targeting the important role that control arms play in ensuring stability and dynamics of vehicles, particularly when electric powertrains are added to chassis platforms created for conventional internal combustion engine (ICE). The study was designed with three phases: Fundamental of control arm dynamics (Phase 1), math formulations into theoretical models (Phase 2) and then experimental validation using the real rail component measurements (Phase 3). Tests were carried out on a straight track at a speed of 15 km/h and 30 km/h targeting the rear axle in an accelerating and the front axle in a braking condition. Results indicated that at 15 km/h, the acceleration of the rear axle was between 0.63 g and 0.49 g whereas at 30 km/h it was between 0.68 g and 0.70 g. During braking at 15 km/h, the front axle's acceleration ranged from a minimum of 0.62 g to a maximum of 0.70 g. At 30 km/h, the acceleration ranged from a minimum of 0.73 g to a maximum of 0.81 g. This suggests that there is a marked disparity in the dynamic action or response of sprung mass and unsprung mass at the different loading conditions. It emphasizes the need for additional support in the control arms and better control over the forces when the electric powertrains will be introduced. All of these have laid a basis for further research aimed at improving the designs of the vehicle structures in advance for the emerging powertrain technologies.

Keywords: Endurance test, Vehicle control arm, Braking test, Accelerating test, Comfort ride

1. Introduction

In the realm of automotive engineering, the suspension system stands as a marvel of design, with the lower and upper control arms at its core. These components, crucial to a vehicle's performance, face a diverse array of forces during various driving conditions—be it riding, accelerating, cornering, or braking. Typically, when consumers consider a vehicle's performance, they focus on horsepower, torque, and zero-to-100 acceleration. However, if control is not maintained, all an engine's power is meaningless. Car engineers initially made strides in power generation to refine suspension systems. Ride comfort and handling are largely governed by the suspension system, its job is to isolate the suspended part of the vehicle from road imperfections and connect that portion with your wheels. The key component needed for this is a structure that can take the energy and send it to the frame without disrupting the entire system [1]–[6].

The system of movable connections that connects the wheels to the vehicle structure and allows relative motion between them is known as the suspension. The interplay between the

suspension system and its hard mounting to the frame are key to ride and handling. In other words, the control arms provide for the vertical displacement of the wheels as to the bodywork and due to this play is very important in terms of driving comfort and handling properties.

The control arms are an important part of the suspension system that in the end help keep a vehicle stable and comfortable. As a vehicle navigates through speed bumps, potholes and other rough patches of road surface mediating forces that travel via the ball joint mechanism through to the control arms. Properly designed and functioning control arms can absorb and dissipate these forces, reducing the risk of vibrations and potential loss of control. Without these critical components, drivers would incur excessive, and detrimental level of vibrations which may be dangerous such as causing the driver to lose control of the vehicle leading into a crash [7], [8].

The suspension system is even more sophisticated, the lower and upper control arms undergo different power in riding, acceleration, turning or braking. The weight and distribution of that weight on the axle is what eventually impacts the ability of these control arms to perform to spec. At A-arm suspensions with unequal-length arms, the upper control arm is usually shorter than the lower arm. This is because this design choice becomes crucial when trying to manage the different forces and weight load characteristics used in order to stabilize a vehicle [9].

As the vehicle transitions through different maneuvers, the force dynamics on these control arms shift, highlighting the critical need for a detailed understanding of their performance under diverse conditions. Poor handling and comfort are caused when weight is not well distributed, and the forces into the control arm of those types create uneasy forces in how a vehicle moves, which makes an analysis of these significant for vehicle safety and performance.

Performance optimization of the vehicle is another important factor. For example, control arms must keep a car under control during various types of driving events — accelerating (including launching), braking and cornering are among the most important. Look at those components in an event model, this analysis helps you to know what they will do under different

conditions and also shows us their weak points where it can improve. This understanding is crucial for improving vehicle dynamics handling, ride comfort and driving experience. Control arms are a major factor in determining a vehicle's ability to control dynamic driving situations and traction, a vital criteria for both normal and performance applications [10].

The analysis of control arms becomes increasingly critical with the adaptation of electric powertrains into chassis platforms originally designed for internal combustion engines (ICE), such as the Volvo XC40 Recharge. The XC40 Recharge is based on the Compact Modular Architecture (CMA) platform shared with conventional versions of the Volvo XC40 [11], [12]. This adaptation introduces unique challenges, particularly regarding the control arms' ability to handle the increased forces associated with electric powertrains. Electric powertrains are capable of providing much higher torque and power outputs compared to their ICE, which stresses the chassis components in a way that they have not been designed for. For instance, the Volvo XC40 Recharge achieves a maximum power output of 300 kW and accelerates from 0 to 100 km/h in just 4.9 seconds. In contrast, the ICE-powered Volvo XC40 produces 183 kW and reaches 100 km/h in 6.4 seconds [13]. This substantial increase in performance places additional demands on the control arms, potentially questioning the reliability of the ICE-designed platform when repurposed for electric power. **Table 1** shows a selection of vehicles from various manufacturers that utilize chassis platforms originally designed for internal combustion engines (ICE) and have been adapted to accommodate electric powertrains.

Thus, evaluating the control arms' performance and durability is essential to ensure that the existing chassis can support the enhanced power and torque of electric vehicles, thereby maintaining safety and reliability across both powertrain types. Therefore, in order to determine the control arm's ability, the load transfer needs to be examined in such a manner that there is a recognized measuring technique that can be done on any vehicle. These two activities, namely, the verification of a strength of a control arm of a vehicle and the analysis of a load vehicle transfer are tightly connected regarding vehicle dynamics and vehicle safety [14], [15].

Table 1. Various electric vehicles that use the ICE platform chassis

Manufacturer	Electric Vehicle	Chassis Platform
Volvo	Volvo XC40	(CMA) platform of ICE version of the Volvo XC40.
Porsche	Porsche Taycan	Chassis platform of Porsche Panamera.
Ford	Ford Mustang Mach-E	Ford CD6 platform initially for Ford Explorer and Ford Mustang.
BMW	BMW i4	G20 platform for BMW 3 Series.
Audi	Audi e-tron	MLB Evo platform for Audi Q7 and Audi Q8.
Mercedes-Bens	Mercedes-Bens EQC	MRA platform originally designed for Mercedes-Benz GLC.
Jaguar	Jaguar I-PACE	Chassis platform of Jaguar PACE and XE.

Load transfer is the redistribution of weight between a vehicle's wheels as it moves, say under conditions of acceleration, braking or turning. It is the change in weight that results from this particular mode of activity which affects how well or poorly even at rest a car behaves on the road. In order to guarantee that the control arms withstood these forces and did not snap, they underwent validation testing which was thorough. It included further simulations and stress testing to ensure that control arms are able to withstand the forces of load shifting without fracturing. Successful vehicle design depends on understanding completely how transfers of load affect suspension components. It also needs to create control arms which maintain the performance and safety of a vehicle in such dynamic environments when these forces are operating [16].

Pachapuri et al. [17] have been investigates the performance and optimization of lower control arms in automotive suspension systems, specifically for a McPherson-type setup. Using Finite Element Analysis (FEA), the study evaluates the forces, stress distribution, and deflection of the lower control arm under various loading conditions, both when stationary and while traversing obstacles at different speeds. The study proved that the use of topology optimization on control arm design can result in considerably lower material consumption, resulting instead in a stronger and lighter control arm. The researchers also recommend more extensive testing on methods of improving control arm movement, which should be based around larger data sets drawn from real life driving situations and varied load conditions. This would encompass trials on different road surfaces in different geographic regions, and load distributions at different driving speeds and under various conditions such as varying road surfaces, driving speeds, and load distributions, to

further validate the control arm's performance and ensure that the optimized design performs reliably in all conditions.

Yu et al. [18] optimized the front suspension lower control arm of an electric SUV, adapting it from a traditional fuel vehicle model to cut development time and costs. A finite element analysis model was used for free modal analysis, identifying bending and torsion as the first two vibration modes with frequencies surpassing the excitation frequency, thus meeting vibration requirements. This was confirmed by a free modal test. The SUV's front suspension dynamics model helped assess the load on the lower control arm, with limit strength analysis showing acceptable stress levels. Multi-disciplinary optimization with Isight achieved a 16.7% mass reduction and improved modal and strength characteristics. However, the tests were conducted under controlled conditions, and real-world variations may affect the lower control arm's performance and reliability. Thus, the reliability of the simulation-based studies and laboratory tests remains uncertain due to their reliance on real world condition impact. Thus, further research work is still needed.

In the present study, this paper presents the investigation of force exerted on the control arm for static and dynamic condition in accelerating and braking by using vehicle dynamic testing. The key insight in this study is that during acceleration, a forward force is applied, causing the vehicle's body to pitch backward and shift more weight to the rear axle. In contrast, braking applies a reverse force, causing the vehicle's body to pitch forward and transfer more weight to the front axle. This weight shift is crucial, as the traction required for both acceleration and braking depends heavily on how the weight is distributed between the front and rear axles. This technical paper is organized into 4 sections as follows: the first section includes an introduction,

a scrutiny of pertinent preliminary work, and previous work on vehicle dynamic testing on control arm development history and the important of this research work. Section two introduces the method to develop the standard vehicle dynamic testing on investigation of control arm and followed by the validation stage of testing method in the third section. The fourth section presents the impact of the testing model in investigation of control arm in vehicle. The conclusion of this study is presented in the last section.

2. Methods

The study was conducted in three phases: Phase 1 focused on the fundamentals of static and dynamic conditions affecting the control arm in the vehicle chassis. Phase 2 involved theoretical analysis through mathematical formulations for both conditions. Phase 3 concentrated on validating these theoretical findings through experimental work. **Figure 1** illustrates the research workflow.

2.1. Theoretical Analysis in Static and Dynamic Condition

The free-body diagram of the isolated part and the surrounding area of the body of the vehicle is shown in **Figure 2**. A free body diagram displays an individual body or a group of bodies along with all the applied forces, moments, and reactions that affect the body. The Free Body Diagram's primary functions are to represent forces and compute reactions. In this study, at low vehicle speeds (below 50 km/h), the effect of wind on acceleration and braking performance is

negligible [19]. At these speeds, the vehicle's inertia and engine output are the primary contributors to performance, while aerodynamic drag due to wind resistance is minimal in comparison to the vehicle's own rolling resistance and mechanical losses.

The normal force under each front (Fz_1) and rear (Fz_2) wheels can be defined as follow:

$$Fz_1 = (1/2)mg(a_2/L) \tag{1}$$

$$Fz_2 = (1/2)mg(a_1/L) \tag{2}$$

Where, m is a mass of the vehicle, g is the gravitational acceleration a_1 is the distance center of gravity (CG) to front axle, a_2 is the distance CG to the rear axle and for wheel base is defined as follow:

$$L = a_1 + a_2 \tag{3}$$

The normal force acting under each tire in static condition is same as Eq. (1) and Eq. (2). The normal force under each front (Fz_1) and rear (Fz_2) wheels in dynamic condition can be defined as:

$$(Fz_1)dyn = -(1/2)mg(h/L) \tag{4}$$

$$(Fz_2)dyn = (1/2)mg(h/L) \tag{5}$$

Where, h is the distance from CG to the road surface. Then, when a car speeding with acceleration, the vertical forces under front and rear wheels can be formulated as:

$$Fz_1 = (1/2)mg(a_2/L) - (1/2)mg(h/L) \tag{6}$$

$$Fz_2 = (1/2)mg(a_1/L) + (1/2)mg(h/L) \tag{7}$$

The force acting on front and rear axle during braking can be defined as:

PHASE 1
Fundamental of static and dynamic condition focusing on control arm in vehicle chassis.

PHASE 2
Theoretical Analysis in Static and Dynamic condition by calculation.

PHASE 3
Validation of force at axle and weight transfer percentage in vehicle chassis.
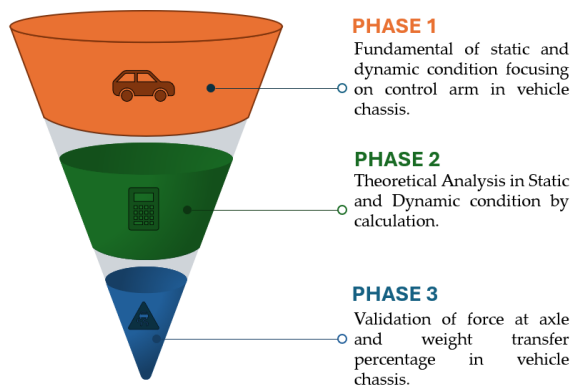
Figure 1. Brief introduction of EDR, as given in the survey
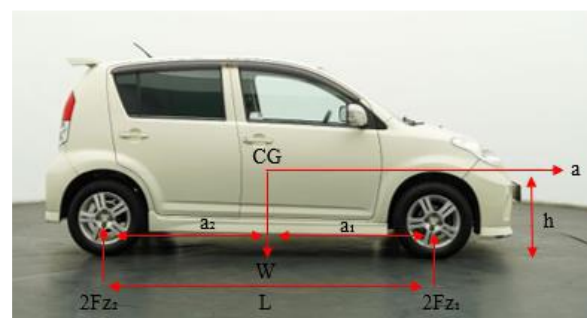
Figure 2. Force acting on the vehicle

$$Fz_1 = (1/2)mg(a_2/L) - Wt \qquad (8)$$

$$Fz_2 = (1/2)mg(a_1/L) + Wt \qquad (9)$$

Where, Wt is the weight transfer during braking and can be defined as:

$$Wt = (A_x mh/L) \qquad (10)$$

Where, A_x is the longitudinal acceleration.

Table 2 shows the parameter of the Perodua Myvi 1.3 L is the selected vehicle that used in this research work. Based on the formula 1 to 10, the force acting on front and rear tires can be calculated and presented in **Table 3**.

2.2. Materials and Procedures

The method for this research work are employs a few component including accelerometer (ADXL335) and arduino UNO acting as the data acquisition (DAQ). Arduino IDE has been used as a cross-platform software to connect between Arduino UNO and accelerometer. In order to measure the weight transfer at front and rear axle, an accelerometer was mounted on the car's sprung and unsprung masses at the front and rear right side [20]–[22]. This method is used to validate the theoretical calculation provided in section 2.1. **Figure 3** and **Figure 4** show the position of the accelerometer attached at body of vehicle.

Prior to installing the accelerometer sensor on the vehicle model, it is crucial to configure the sensor properly to ensure accurate data collection. Calibration of the accelerometer is required to confirm that it covers the correct range of vehicle acceleration. Under static conditions, the accelerometer should ideally measure 1 g (1 gravitational force), which is equal to Earth's gravitational acceleration of 9.81 m/s². When aligned parallel to gravity along the z-axis, the z-axis output should theoretically measure 9.81 m/s². Tilting the sensor in one direction will cause the output voltage to increase, while tilting it in the opposite direction will cause it to decrease. Accelerometers are most sensitive to small changes in tilt when positioned parallel to Earth's gravity, allowing for precise measurements. However, beyond approximately 45 degrees of tilt, the sensitivity decreases. The Arduino IDE code used for the accelerometer can be found in Appendix 1.

The test procedure was conducted on a test track at speeds of 15 km/h and 30 km/h. These speeds were chosen to cover a broad spectrum of operating parameters and accurately reflect real-world driving conditions. The experiments were carried out on a straight track located within the university building (see **Figure 5**). Testing was performed at both 15 km/h and 30 km/h on a typical dry road surface. Each test was repeated five times to ensure comprehensive data collection and analysis.

Table 2. Perodua Myvi 1.3L parameter

Parameter	Symbol	Value and Unit
Kerb weight	-	955 kg
Kerb weight + load	m	1085 kg
Wheelbase	L	2440 mm
Length from the center of gravity to the front axle	a_1	976 mm
Length from the center of gravity to the rear axle	a_2	1464 mm
Height from center of gravity to the ground	h	610 mm
Track width	B	1455 mm
Turning radius	R	7 m
Lateral acceleration	a_x	9.913 m/s²
Speed	v	8.33 m/s
Acceleration	a	2.15 m/s²
Gravity acceleration	g	9.81 m/s

Table 3. Force acting on front and rear tires

Vehicle Condition	Front tire Force (N)	Rear Tire Force (N)
Static	3193.2	2128.8
Accelerating	2901.6	2420.4
Braking	1064.4	5321.9

(a)   (b)
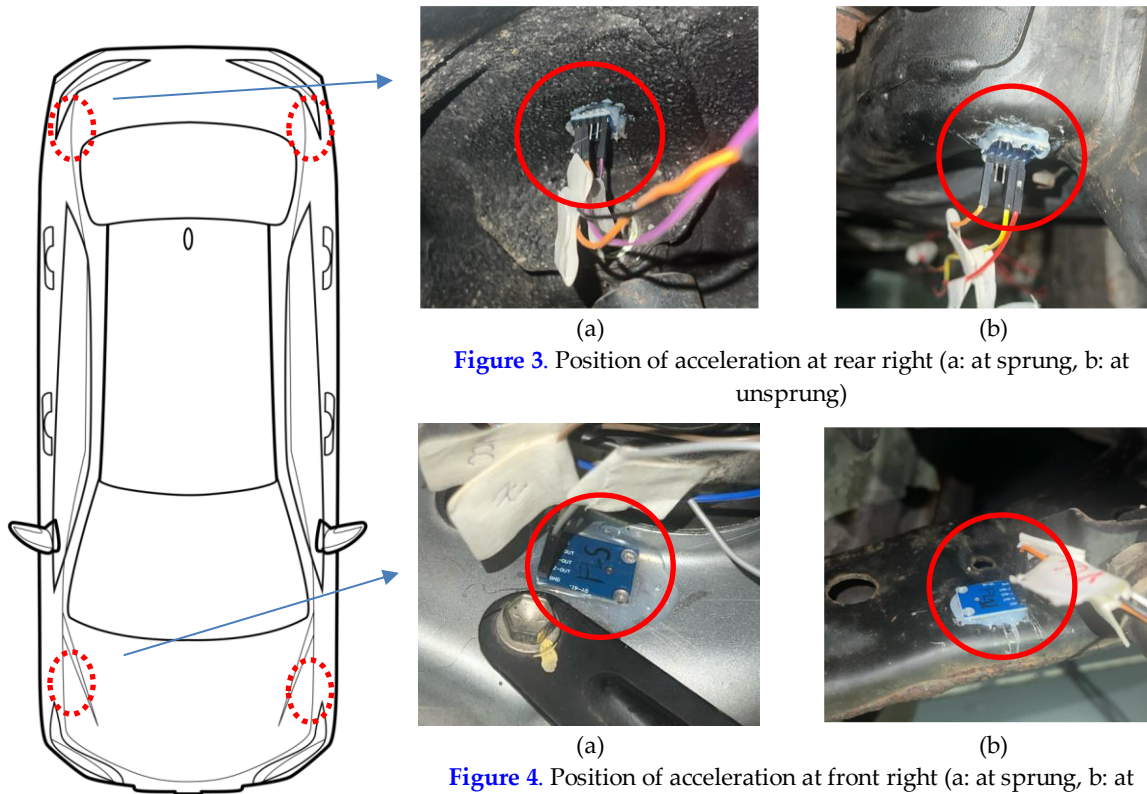
Figure 3. Position of acceleration at rear right (a: at sprung, b: at unsprung)

(a)   (b)

Figure 4. Position of acceleration at front right (a: at sprung, b: at unsprung
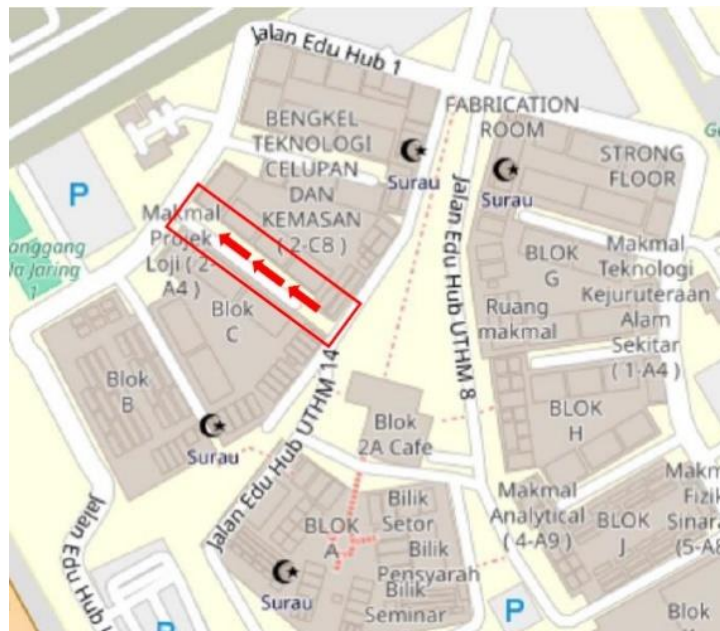
Figure 5. The location of road selection at UTHM Campus Pagoh

3. Results and Discussion

A scenario including acceleration and braking at two distinct speeds 15 km/h and 30 km/h was used for the investigation. The purpose of the two-speed study was to examine how vehicle speed affects weight transfer to the front and rear axles. Weight shifts from the front to the back axle during acceleration and from the back to the front axle when braking, as was previously established. As a result, in this part, the outcome will only be focused on the rear axle when accelerating, and the front axle when braking.

Figure 6 presents the rear axle acceleration of a vehicle during acceleration, recorded at two distinct speeds: 15 km/h and 30 km/h. These measurements are taken from both sprung and
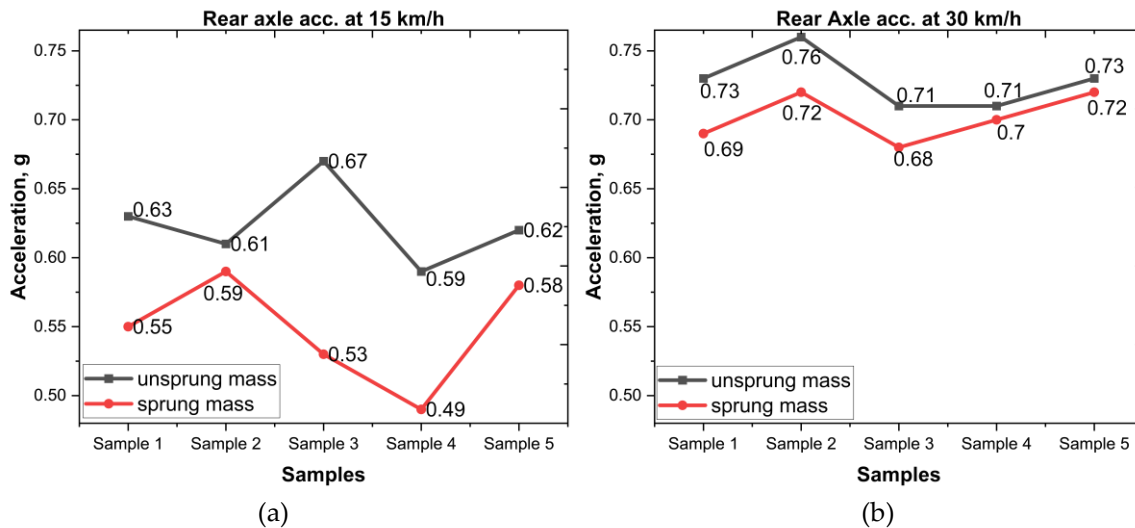
Figure 6. Rear axle acceleration during vehicle accelerate

unsprung masses to assess the dynamic behavior under acceleration forces. For analysis at 15 km/h, the acceleration observed in the sprung mass shows minor fluctuations, beginning at 0.55 g, peaking at 0.67 g in Sample 3, and then decreasing to 0.58 g by Sample 5. The variability suggests a significant response to acceleration forces, likely due to weight transfer and chassis dynamics as the vehicle speeds up. For unsprung mass, a more pronounced variance in acceleration values is noted, ranging from 0.63 g to 0.49 g. The lowest value at Sample 4 suggests that the unsprung mass, including components like the control arm, experiences significant strain under dynamic load variations at this speed.

For analysis at 30 km/h, the pattern of sprung mass is more consistent, starting at 0.69 g, with a slight rise to 0.76 g, and tapering off back to 0.73 g. The higher overall values compared to 15 km/h indicate that as speed increases, the sprung mass experiences greater dynamic forces, stressing the importance of robust chassis design for high-speed maneuvers. For unsprung mass, like the 15 km/h data, the unsprung mass shows a range from 0.68 g to 0.70 g. The smaller range of variation at this higher speed could suggest a stabilization effect on the unsprung components due to increased gyroscopic forces and faster reaction times of the suspension system.

These findings highlight the critical role of vehicle dynamics in the design and sustainability of ICE chassis platforms, particularly when adapted for electrified powertrains. The data shows the difference in the effect of acceleration on the sprung and unsprung masses which is fundamental toward the design of suspension components and control arms in maintaining vehicle control and stability. The drastic reduction of the unsprung mass acceleration at lower velocities (15 km/h) also highlights probable areas of improvement in the damping of the suspension systems and the strength of the control arms in managing dynamic loads, especially in electric vehicle conversions, where weight distribution may widely differ from the conventional ICE vehicles [23].

The increased load and stress on the control arms suggest a need for reinforced materials or innovative designs that can absorb and redistribute these forces more efficiently. Also, the high variability in unsprung mass acceleration underscores the importance of enhancing the shock-absorbing capabilities of the vehicle's suspension system to prevent wear and tear and improve vehicle stability.

The graphs in **Figure 7** illustrate two additional cases of front axle acceleration during braking — one recorded at a speed of 15 km/h and the other recorded at 30 km/h and data are sorted by their sprung/unsprung mass condition, showing different dynamic behaviors of the sprung/unsprung masses for brake application lines. Automotive engineers would benefit greatly by analysing these results particularly as it relates to weight transfer and the stability of a vehicle that integrates electric powertrains. At 15 km/h the sprung mass accelerations oscillate somewhere between a peak of 0.61 to 0.66 g during the analysis phase. The little oscillations are expected to indicate a maneuver where the sprung weight
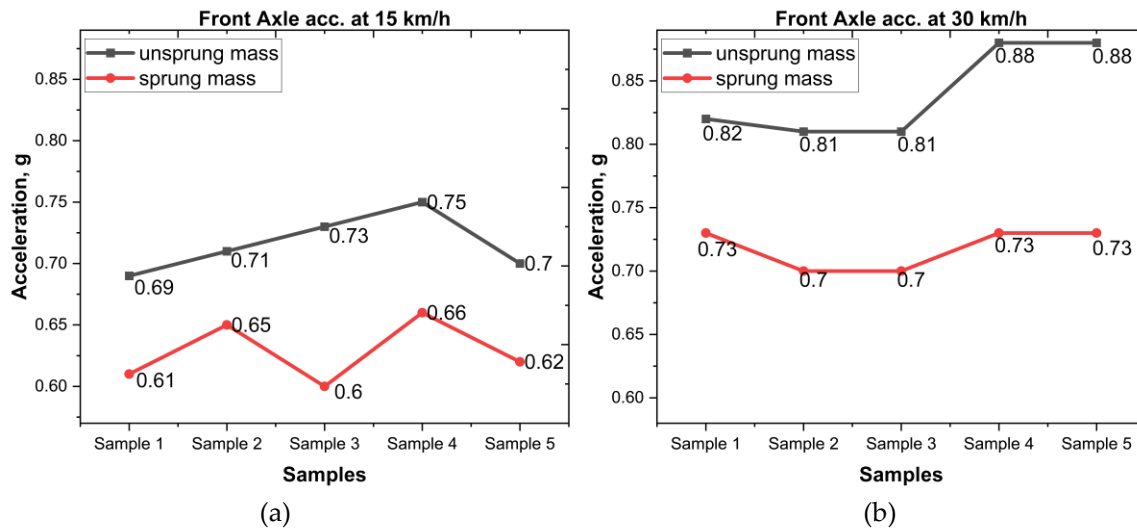
Figure 7. Front axle acceleration during vehicle braking

undergoes large load migration during low-speed braking (low inertial scrub force) duties. It might be due to transfer of weight from the rear axle to the front, which affects vehicle balance during deceleration. For unsprung mass, consisting of components such as control arms and suspension parts, displays a broader range of acceleration, from 0.69 g to 0.75 g. The peaks observed in Samples 3 and 5 (0.73 g and 0.75 g) indicate higher load concentrations on the unsprung components, which can be a key factor in determining the durability and design robustness of the control arms under braking stress.

At the higher speed of 30 km/h, shows that the acceleration values for the sprung mass remain consistent at around 0.73 g which suggests that even during heavy braking, when the forces under consideration would be greater, the car's suspension system is able to control that weight transfer effectively and thus provide stability in both normal as well as emergency stops with minimal chance of wheel lockup. This suggests a well-sorted chassis that is durable enough to handle the added brake force without invoking the masses. Conversely unsprung mass experiences an acceleration range that spike to much higher accelerations (approximately 0.81 g - 0.88 g). The peaks in Sample 2 (0.88 g) and Sample 5 (0.88g), showcase the greater load exerted upon suspension components under deceleration at relatively quicker velocities. This suggests that as braking force increases, more stress is placed on the control arms and other unsprung components, necessitating a robust design to handle these peak loads without compromising structural integrity.

The comparison between the two speeds reveals several important dynamics in the weight transfer process during braking. At lower speeds, it shows that there is a greater fluctuation in both sprung and unsprung mass accelerations, implying more frequent load shifts that can affect handling and comfort. However, at higher speeds, the sprung mass shows more stability, while the unsprung mass experiences higher stress.

Such conclusions are of great importance for the design and sustainability of ICE chassis platforms, especially the designs that are modified for integration of electric powertrains. The higher forces on the unsprung mass during braking at 30 km/h illustrates the demand for tailored and strengthened suspension system as well as control arm elements. Electric vehicles that will be utilizing different weight distribution from the placement of the batteries will cause different stress patterns therefore the necessity to revisit control arm designs on such platforms. These are very useful for building control arms and suspension systems that can support the different forces produced when electric powertrains are incorporated [24].

The results of comparing calculated and experimental data for each axle, under both acceleration and braking conditions at a speed of 30 km/h, are presented in **Table 4**. Experimental data values are incorporated into Eqs. (6) and (7) for acceleration, and Eqs. (8) and (9) for braking conditions. **Table 4** also shows the force acting on the axle, calculated using the maximum acceleration values obtained from 5 samples.

From **Table 4**, the percentages of weight transfer can be computed based on equation 10. The percentage of weight transfer under braking and acceleration conditions for experiment result at speed of 30 km/h in **Table 5**. Under acceleration, the front axle's weight transfer percentage is 40.4%, while the rear axle's weight transfer percentage is 59.6%. Weight transfer is 2.8% at the rear axle and 97.2% at the front axle when the vehicle is braking. The front axle produced the greatest force during the braking situation based on the proportion of weight transfer. The performance of the lower arm is of the utmost importance in this situation.

Table 4. Comparison of calculation and experimental each axle data

Vehicle Condition	Axle	Experimental		Calculation	Percentages error (%)
		15 km/h	30 km/h	30 km/h	30 km/h
Acceleration	Front	5279.4	4300.3	3249.3	-24.4
	Rear	5364.5	6343.6	7394.6	14.2
Braking	Front	9004.9	10345.6	9523.3	-8.6
	Rear	1639.16	298.22	10345.6	97.1

Table 5. Percentage of weight transfer

Vehicle Condition	Axle	Weight Transfer (%)
		30 km/h
Acceleration	Front	40.4
	Rear	59.6
Braking	Front	97.2
	Rear	2.8

4. Conclusion

The goal of this research was to investigate the force exerted on the control arm for static and dynamic condition in accelerating and braking by using vehicle dynamic testing. This study utilized an accelerometer and Arduino UNO for the testing. Each condition (acceleration and braking) was tested five times under controlled weather and road conditions in a straight line. The results emphasize the critical importance of monitoring unsprung mass during high-speed braking, particularly for integrating electric powertrains. Electric vehicles, with their distinct weight distribution, may amplify the forces on the suspension system during braking. Consequently, the findings underscore the necessity for more robust control arms and suspension designs to manage increased dynamic loads while maintaining ride quality and safety. This research lays the groundwork for future studies aimed at optimizing vehicle structures to accommodate new powertrain technologies without sacrificing performance or safety.

Author's Declaration

Authors' contributions and responsibilities

Nuurshafiqah Anuar (Wrote the original paper; Data Curation), Syabillah Sulaiman (Funding acquisition; Visualisation; Conseptualization; Supervision), Muhamad Asri Azizul (Wrote the revised manuscript; Data Curation;Visualization; Conseptualization), Shaiful Fadzil Zainal Abidin (Review and revised manuscript; Data Interpretation), Noririda Mohamed (Conseptualization; Review and editing manuscript), Rahmah Mahmudin (Visualisation; Supervision), Norhasikin Ismail (Formal analysis; Conceived and designed the experiments).

Availability of data and materials

All data are available from the authors.

Competing interests

The authors declare no competing interest.

Additional information

No additional information from the authors.
_____

References

[1] W. Hou, X. Yang, W. Zhang, and Y. Xia, "Design of energy-dissipating structure with functionally graded auxetic cellular material," *International Journal of Crashworthiness*, vol. 23, no. 4, pp. 366–376, Jul. 2018, doi: 10.1080/13588265.2017.1328764.

[2] F. Xu, X. Zhang, and H. Zhang, "A review on functionally graded structures and materials for energy absorption," *Engineering Structures*, vol. 171, pp. 309–325, 2018, doi: 10.1016/j.engstruct.2018.05.094.

[3] C. W. Isaac and C. Ezekwem, "A review of the crashworthiness performance of energy absorbing composite structure within the context of materials, manufacturing and maintenance for sustainability," *Composite Structures*, vol. 257, p. 113081, 2021, doi: 10.1016/j.compstruct.2020.113081.

[4] M. R. Abd - Elwahab, A. O. Moaaz, W. F. Faris, N. M. Ghazaly, and M. M. Makrahy, "Evaluation the New Hydro-Pneumatic Damper for Passenger Car using LQR, PID and H-infinity Control Strategies," *Automotive Experiences*, vol. 7, no. 2, pp. 207–223, Aug. 2024, doi: 10.31603/ae.10796.

[5] R. P. Putra *et al.*, "Design and Crash Test on a Two-Passenger City Car Frame using Finite Element Method," *Automotive Experiences*, vol. 7, no. 2, pp. 270–283, Sep. 2024, doi: 10.31603/ae.11306.

[6] A. R. Zubir, K. Hudha, Z. A. Kadir, and N. H. Amer, "Enhanced Modeling of Crumple Zone in Vehicle Crash Simulation Using Modified Kamal Model Optimized with Gravitational Search Algorithm," *Automotive Experiences*, vol. 6, no. 2, pp. 372–383, Aug. 2023, doi: 10.31603/ae.9289.

[7] U. Ö. Demli and E. Acar, "Design optimization of armored wheeled vehicle suspension lower control arm," *Materials Testing*, vol. 64, no. 7, pp. 932–944, Jul. 2022, doi: 10.1515/mt-2021-2154.

[8] A. Messana, "Suspension lower control arm case study: enhancing lightweight and vibration reduction," *Polytechnico di Torino, Turin, Italy*, 2019.

[9] P. Upadhyay, M. Deep, A. Dwivedi, A. Agarwal, P. Bansal, and P. Sharma, "Design and analysis of double wishbone suspension system," *IOP Conference Series: Materials Science and Engineering*, vol. 748, no. 1, p. 012020, Feb. 2020, doi: 10.1088/1757-899X/748/1/012020.

[10] J. Chen, Z. Liu, S. Chen, B. Peng, and A. Tang, "Lightweight Design and Multi-Objective Optimization for a Lower Control Arm Considering Multi-Disciplinary Constraint Condition," Apr. 2019, doi: 10.4271/2019-01-0822.

[11] H. Hassan and M. Ibrahim, "Flexibility of platforms and its impact on platforms lifecycle: a review and a focused case," 2021.

[12] I. Andersson and J. Oddeby, "Development of Wireless Charging Component in Vehicle," 2018.

[13] G. Lye, "Volvo XC40 officially revealed – CMA platform, Drive-E engines, first model offered in 'Care by Volvo' service," Cars International News, Sep. 21, 2017.

[14] M. Abebe and B. Koo, "Fatigue Life Uncertainty Quantification of Front Suspension Lower Control Arm Design," *Vehicles*, vol. 5, no. 3. pp. 859–875, 2023, doi: 10.3390/vehicles5030047.

[15] D. C. Barton and J. D. Fieldhouse, "Vehicle Structures and Materials," in *Automotive Chassis Engineering*, Springer, 2024, pp. 257–297.

[16] M. Carello, H. de Carvalho Pinheiro, A. Messana, A. Freedman, A. Ferraris, and A. G. Airale, "Composite Control Arm Design: A Comprehensive Workflow," *SAE International Journal of Advances and Current Practices in Mobility*, vol. 3, no. 5, pp. 2021-01–0364, Apr. 2021, doi: 10.4271/2021-01-0364.

[17] M. S. A. Pachapuri, R. G. Lingannavar, N. K. Kelageri, and K. K. Phadate, "Design and analysis of lower control arm of suspension system," *Materials Today: Proceedings*, vol. 47, pp. 2949–2956, 2021, doi: 10.1016/j.matpr.2021.05.035.

[18] Z. Yu, H. Jia, and X. Huang, "Design of the Lower Control Arm of an Electric SUV Front

Suspension Based on Multi-Disciplinary Optimization Technology.," *Jordan Journal of Mechanical & Industrial Engineering*, vol. 15, no. 1, 2021.

[19] S. Heydari, P. Fajri, N. Lotfi, and B. Falahati, "Influencing Factors in Low Speed Regenerative Braking Performance of Electric Vehicles," in *2018 IEEE Transportation Electrification Conference and Expo (ITEC)*, 2018, pp. 494–499, doi: 10.1109/ITEC.2018.8450260.

[20] Z. Wang, M. Li, and H. Wang, "Vehicle Mass Identification Based on Two-axle and Two-mass Vibration Model," *IOP Conference Series: Materials Science and Engineering*, vol. 787, no. 1, p. 012024, Mar. 2020, doi: 10.1088/1757-899X/787/1/012024.

[21] K. Prażnowski, J. Mamala, A. Deptuła, A. M. Deptuła, and A. Bieniek, "Diagnosis of the Pneumatic Wheel Condition Based on Vibration Analysis of the Sprung Mass in the Vehicle Self-Diagnostics System," *Sensors*, vol. 23, no. 4. 2023, doi: 10.3390/s23042326.

[22] P. Krauze, J. Kasprzyk, and J. Rzepecki, "Experimental attenuation and evaluation of whole body vibration for an off-road vehicle with magnetorheological dampers," *Journal of Low Frequency Noise, Vibration and Active Control*, vol. 38, no. 2, pp. 852–870, Jul. 2018, doi: 10.1177/1461348418782166.

[23] K. V. Singh, H. O. Bansal, and D. Singh, "A comprehensive review on hybrid electric vehicles: architectures and components," *Journal of Modern Transportation*, vol. 27, no. 2, pp. 77–107, 2019, doi: 10.1007/s40534-019-0184-3.

[24] N. R. Dhivare and K. P. Kolhe, "Vibration Analysis and Optimization of Upper Control Arm of Light Motor Vehicle Suspension System," *International Journal for Innovation Research in Science and Technology*, vol. 3, no. 02, 2016.

Appendix
Appendix 1

```
1   #include <Wire.h>
2
3   const int strainPin = A5;        // Analog pin connected to the strain gauge
4   const float vRef = 5.0;          // Voltage reference of the microcontroller (5V for most Arduinos)
5   const float sensitivity = 2.0;   // Sensitivity of the BF-350 strain gauge in mV/V
6   const float excitationVoltage = 5.0;    // Excitation voltage for the Wheatstone bridge
7   const float armLength = 0.2;     // Length of the lower arm in meters (adjust based on your setup)
8   const float gravity = 9.81;      // Acceleration due to gravity in m/s^2
9
10  const int MPU_ADDR = 0x58;
11
12  int16_t accelerometer_x, accelerometer_y, accelerometer_z;
13  int16_t gyro_x, gyro_y, gyro_z;
14  int16_t temperature;
15
16  char tmp_str[7];
17
18  float accel_sensitivity = 16384.0; // Sensitivity for the accelerometer: 16384 LSB/g
19  float gyro_sensitivity = 131.0;    // Sensitivity for the gyroscope: 131 LSB/(°/s)
20
21  char* convert_int16_to_str(int16_t i) {
22    sprintf(tmp_str, "%6d", i);
23    return tmp_str;
24  }
25
26  int zpin1 = A0;
27  int zvalue1;
28
29  int zpin2 = A1;
30  int zvalue2;
31
32  int zpin3 = A2;
33  int zvalue3;
34
35  int zpin4 = A3;
36  int zvalue4;
37
38  void setup() {
39    Serial.begin(9600);
40    Wire.begin();
41    Wire.beginTransmission(MPU_ADDR);
42    Wire.write(0x6B);
43    Wire.write(0);
44    Wire.endTransmission(true);
45  }
46
47  void loop() {
48    // Read values from analog sensors
49    zvalue1 = analogRead(zpin1);
50    int z1 = map(zvalue1, 277, 410, -100, 100);
51    float zg1 = (float)z1 / (-100.00);
52
53    zvalue2 = analogRead(zpin2);
54    int z2 = map(zvalue2, 277, 410, -100, 100);
55    float zg2 = (float)z2 / (-100.00);
```

```
57    zvalue3 = analogRead(zpin3);
58    int z3 = map(zvalue3, 277, 410, -100, 100);
59    float zg3 = (float)z3 / (-100.00);
60
61    zvalue4 = analogRead(zpin4);
62    int z4 = map(zvalue4, 277, 410, -100, 100);
63    float zg4 = (float)z4 / (-100.00);
64
65    // Read values from MPU6050
66    Wire.beginTransmission(MPU_ADDR);
67    Wire.write(0x3B);
68    Wire.endTransmission(false);
69    Wire.requestFrom(MPU_ADDR, 7 * 2, true);
70
71    accelerometer_x = Wire.read() << 8 | Wire.read();
72    accelerometer_y = Wire.read() << 8 | Wire.read();
73    accelerometer_z = Wire.read() << 8 | Wire.read();
74    temperature = Wire.read() << 8 | Wire.read();
75    gyro_x = Wire.read() << 8 | Wire.read();
76    gyro_y = Wire.read() << 8 | Wire.read();
77    gyro_z = Wire.read() << 8 | Wire.read();
78
79    // Convert raw values to meaningful units
80    float accel_x = accelerometer_x / accel_sensitivity;
81    float accel_y = accelerometer_y / accel_sensitivity;
82    float accel_z = accelerometer_z / accel_sensitivity;
83
84    float gyro_x_dps = gyro_x / gyro_sensitivity;
85    float gyro_y_dps = gyro_y / gyro_sensitivity;
86    float gyro_z_dps = gyro_z / gyro_sensitivity;
87
88    // Calculate strain and other values from the strain gauge
89    int rawValue = analogRead(strainPin);
90    float voltage = (rawValue / 1023.0) * vRef;
91    float strain = (voltage / excitationVoltage - 0.5) * sensitivity;
92    float calibrationFactor = 10.0;   // Adjust this based on your calibration
93    float force = strain * calibrationFactor;
94    float torque = force * armLength;
95    float weight = torque / gravity;
96
97    // Print out data
98    Serial.print("Analog Sensors: ");
99    Serial.print(zg1);
100   Serial.print("\t");
101   Serial.print(zg2);
102   Serial.print("\t");
103   Serial.print(zg3);
104   Serial.print("\t");
105   Serial.print(zg4);
106   Serial.println("g");
```

```
107
108    Serial.print("MPU6050 Data: ");
109    Serial.print("aX = ");
110    Serial.print(accel_x);
111    Serial.print(" | aY = ");
112    Serial.print(accel_y);
113    Serial.print(" | aZ = ");
114    Serial.print(accel_z);
115    Serial.print(" | tmp = ");
116    Serial.print(temperature / 340.00 + 36.53);
117    Serial.print(" | gX = ");
118    Serial.print(gyro_x_dps);
119    Serial.print(" | gY = ");
120    Serial.print(gyro_y_dps);
121    Serial.print(" | gZ = ");
122    Serial.println(gyro_z_dps);
123
124    Serial.print("Strain Gauge Data: ");
125    Serial.print("Raw Value: ");
126    Serial.print(rawValue);
127    Serial.print("\tVoltage: ");
128    Serial.print(voltage, 4);
129    Serial.print(" V\tStrain: ");
130    Serial.print(strain, 4);
131    Serial.print("\tForce: ");
132    Serial.print(force, 4);
133    Serial.print(" N\tTorque: ");
134    Serial.print(torque, 4);
135    Serial.print(" Nm\tWeight: ");
136    Serial.print(weight, 4);
137    Serial.println(" kg");
138
139  delay(500);
140  }
```